

A Wavelet-based Stereo Matching Framework for Solving Frequency Convergence Inconsistency

Xiaobao Wei^{1,2}, Jiawei Liu^{1,3,4*}, Dongbo Yang^{1,3,4,7}, Junda Cheng⁵, Changyong Shu⁶, Wei Wang^{1,3,4}

¹Shenyang Institute of Automation, Chinese Academy of Sciences

²Nanjing University of Science and Technology, ³Liaoning Liaohe Laboratory

⁴Key Laboratory on Intelligent Detection and Equipment Technology of Liaoning Province

⁵Huazhong University of Science and Technology, ⁶Beihang University

⁷University of Chinese Academy of Sciences

wxb@njust.edu.cn, liujiawei@sia.cn

Abstract

We find that the EPE evaluation metrics of RAFT-stereo converge inconsistently in the low and high frequency regions, resulting high frequency degradation (e.g., edges and thin objects) during the iterative process. The underlying reason for the limited performance of current iterative methods is that it optimizes all frequency components together without distinguishing between high and low frequencies. We propose a wavelet-based stereo matching framework (Wavelet-Stereo) for solving frequency convergence inconsistency. Specifically, we first explicitly decompose an image into high and low frequency components using discrete wavelet transform. Then, the high-frequency and low-frequency components are fed into two different multi-scale frequency feature extractors. Finally, we propose a novel LSTM-based high-frequency preservation update operator containing an iterative frequency adapter to provide adaptive refined high-frequency features at different iteration steps by fine-tuning the initial high-frequency features. By processing high and low frequency components separately, our framework can simultaneously refine high-frequency information in edges and low-frequency information in smooth regions, which is especially suitable for challenging scenes with fine details and textures in the distance. Extensive experiments demonstrate that our Wavelet-Stereo outperforms the state-of-the-art methods and ranks 1st on both the KITTI 2015 and KITTI 2012 leaderboards for almost all metrics. We will provide code and pre-trained models to encourage further exploration, application, and development of our innovative framework (<https://github.com/SIA-IDE/Wavelet-Stereo>).

1 Introduction

Stereo matching aims to estimate dense disparity maps by matching corresponding pixels between rectified stereo images. This technique serves as the cornerstone for autonomous driving [48], augmented reality [49], and robotic manipulation [18]. Despite decades of research, achieving high-precision and high-efficiency stereo matching remains challenging.

The advent of deep learning has revolutionized the field enabling end-to-end disparity prediction through CNNs [9, 12, 17, 24, 29, 39, 40]. Aggregation-based methods [3, 21, 34, 46] improve accuracy by building 4D correlation volumes and applying 3D convolutions for regularization. To avoid expensive 3D convolution, RAFT-stereo [25] updates the disparity map and hidden states by iteratively indexing from the all-pairs correlation volume and using the gate recursive unit operator. Subsequent RAFT-based iterative methods [13, 22, 25, 37, 43, 51] suffer from the issue that

*Corresponding author.

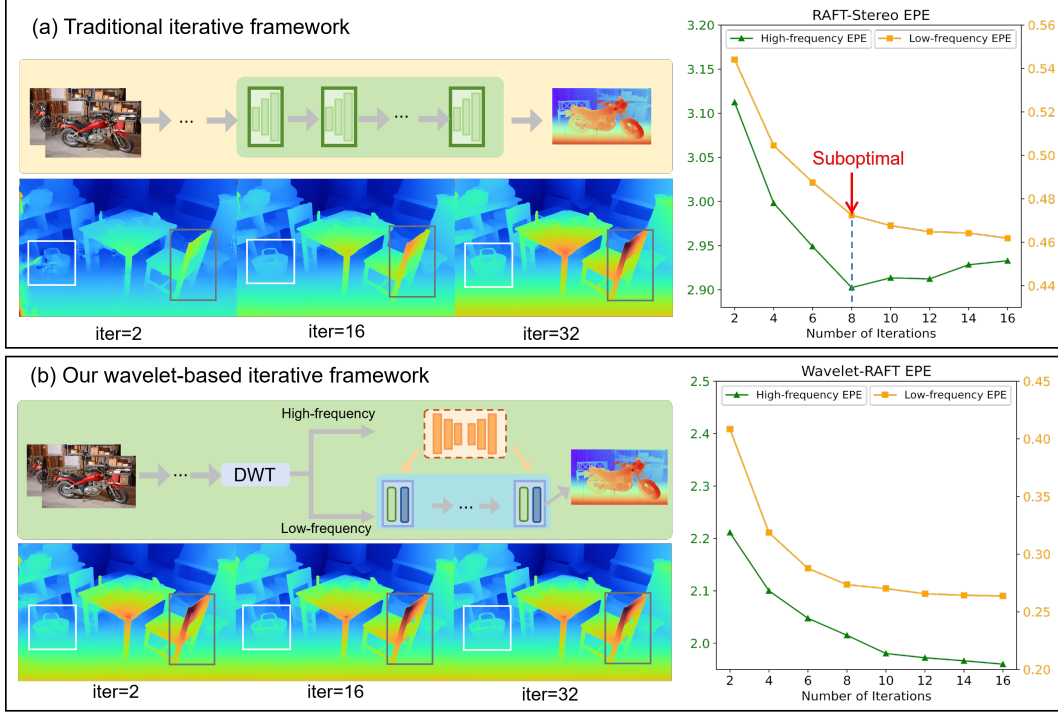


Figure 1: High and low frequency region EPE performance evaluation for some challenging scenes on ETH3D dataset [33]. (a) Traditional iterative-based methods [25] process the all frequency components uniformly, resulting in inconsistent convergence in different frequency regions. (b) We design frequency-specific feature extraction and processing modules to achieve overall optimization for different frequency components.

correlation volume contains significant redundant noise, resulting high frequency degradation (e.g., edges and thin objects [37, 43, 51]) during the iterative process. To address this, Selective-Stereo [37] employs variable receptive fields instead of a fixed one in the GRU to better capture high-frequency information, while DLNR [51] replaces the GRU with an LSTM to retain more high-frequency information. However, these methods [37, 51] do not explain clearly why the frequency degradation phenomenon occurs during the iteration process.

We present the frequency convergence result of RAFT-stereo [25] by calculating the EPE evaluation metric for both high-frequency and low-frequency regions. Fig. 1 (a) shows that the phenomenon of **frequency convergence inconsistency**, i.e., different frequency components exhibit different convergence behaviors. The underlying reason for the limited performance of iterative methods is that it jointly optimizes “all frequency components” using a single GRU update operator, without distinguishing between high and low frequencies. In this paper, **we introduce wavelets into stereo matching (Wavelet-Stereo) by explicitly decomposing the high-frequency and low-frequency components via discrete wavelet transform** as shown in Fig. 1 (b), so that high and low-frequency features can be extracted and processed separately according to different frequency properties.

Specifically, we first explicitly decompose an image into high and low frequency components using the Haar wavelet [31]. Then, we use two frequency feature extractors to extract multi-scale high-frequency features and low-frequency features separately. Finally, we propose a novel **high-frequency preservation update operator (HPU)** to simultaneously refines high-frequency information in edges and low-frequency information in smooth regions. The proposed HPU contains two modules: (1) An iterative-based frequency adapter can provide adaptive refined high-frequency features at different iteration steps by fine-tuning the initial high-frequency features. (2) A high-frequency preservation LSTM ensures that high-frequency information is not lost and also provides detailed texture information to guide low-frequency updates. Our novel components can be plug-and-played into multiple iterative-based methods. Extensive experiments demonstrate that our Wavelet-Stereo outperforms the state-of-the-art methods and ranks 1st **on both the KITTI 2015 and KITTI 2012**

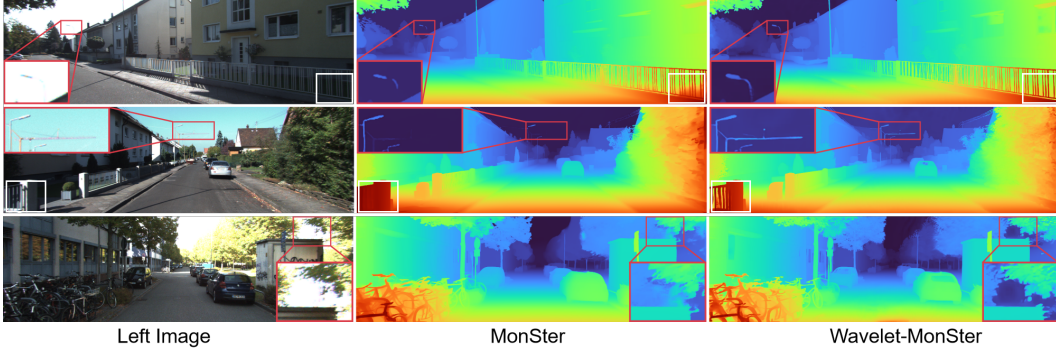


Figure 2: **Visual comparison on KITTI.** All models are trained on Scene Flow and tested directly on KITTI [15, 28]. Wavelet-MonSter outperforms MonSter in challenging areas with high-frequency details, fine structures.

leaderboards for almost all metrics. Our framework can handle challenging scenes with fine details and textures in the distance, as show in Fig.2.

2 Related Work

Aggregation-based methods in Stereo Matching. Aggregation-based methods [3, 7, 8, 17, 21, 35, 44, 45, 46, 50] have shown significantly improvement in accuracy and robustness. GCNet [21] a 4D correlation volume by concatenating the left and right feature maps within a predefined disparity search range, followed by cost aggregation using 3D convolutions to generate the final matching results. To avoid the use of 3D convolution, AANet [46] introduces intra-scale and cross-scale cost aggregation to capture the edge and non-edge area. ACVNet [41] propose the attention concatenation volume to eliminate noise in the cost volume and improve the performance in the ambiguous region. While aggregation-based methods achieve competitive accuracy, their computational overhead remains prohibitive for being applied to high-resolution inputs.

Iterative-based methods in Stereo Matching. Iterative-based methods [5, 11, 13, 19] have demonstrated significant advantages over aggregation-based methods. RAFT-Stereo [25] introduces an all-pairs correlation volume pyramid and utilizes GRU-based update operators to perform iterative disparity updates. On this basis, IGEV-Stereo [43] addresses the issue that the initial correlation volume is excessively coarse by a lightweight cost aggregation network before iteration. CREStereo [22] proposes a adaptive group correlation layer, computes correlations within local search windows to reduce memory and computational overhead. These methods suffer from slow convergence due to their inability to effectively coordinate the refinement of high and low frequency region.

Frequency-based methods in Stereo Matching. Although frequency domain information [4, 14, 30, 47] has been widely applied in computer vision tasks, its utilization in the field of stereo matching remains relatively limited. Selective-Stereo [37] proposes a selective recurrent unit module to adaptively captures multi-frequency information. This data-driven frequency separation methods lack interpretability in their learned decomposition patterns and demonstrate limited generalization capability across diverse datasets. DLNR [51] decouples the hidden state from the update matrix of disparity map and transfers high-frequency across iteration. However, it just defines the hidden state as a high-frequency feature which lacks a clear physical definition.

3 Methodology

For iterative-based stereo matching frameworks, the correlation volume C is provided as a condition to the update operator, which predicts a series of disparity fields $\{d_1, \dots, d_{n_k}\}$ from a pair of rectified images $(I_L, I_R \in \mathbb{R}^{H \times W \times 3})$ by using the current estimate of disparity d_k to index the correlation volume C . In fact, the correlation volume containing considerable noisy information is used to predict d_k , causing the hidden state to lose critical information during the iteration process. For example, the hidden state increasingly contain global low-frequency information while losing local high-frequency information such as edges and thin objects [37, 43, 51]. Therefore, we introduce wavelets into

stereo matching (Wavelet-Stereo) and propose a novel high-frequency preservation update (HPU) operator containing two modules: (1) An iterative-based frequency adapter can provide adaptive refined high-frequency features at different iteration steps by fine-tuning the initial high-frequency features F_h extracted by a high-frequency feature extractor E_h . (2) A high-frequency preservation LSTM ensures that high-frequency information is not lost and also provides updated high-frequency guidance for updating the hidden state.

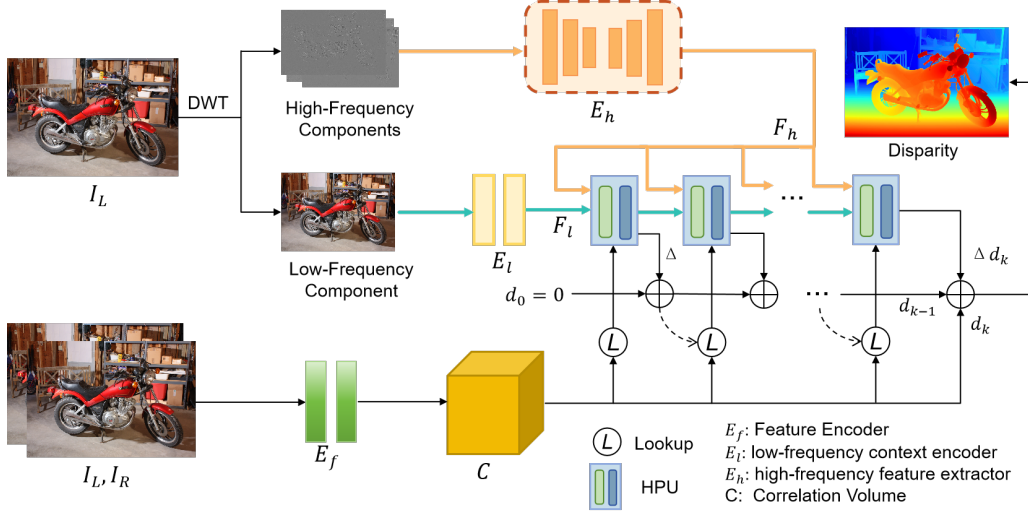


Figure 3: **Overview of Wavelet-RAFT.** Wavelet-RAFT employs a dual-branch architecture comprising: (1) a dedicated feature extraction branch for capturing high-frequency texture features E_h , (2) a update branch that progressively refines structural information. The aggregated high-frequency features F_h serve as guidance information injected into the High-frequency Preservation Update (HPU) operator to update the hidden states during each iteration.

3.1 Overall Pipeline

Since our method can be integrated into any iterative-based methods, we use Wavelet-RAFT as a representative example to demonstrate the key innovations of our framework, employing the same feature extraction network E_f and cost-volume construction as RAFT-Stereo [25] is used. As shown in Fig. 3, our framework consists of three steps: (1) Frequency decomposition: We explicitly separate high-frequency and low-frequency components by discrete wavelet transform in Section 3.2. (2) Frequency Feature Extraction: we extract multi-scale high-frequency features and low-frequency features separately in Section 3.3. (3) Iterative updating: we propose a novel update operator using high-frequency features as conditions to guide each iterative process in Section 3.4.

3.2 Frequency Decomposition

We use the Haar wavelet [31] to decompose the left image I_L into four sub-images I_{sub} with low and high frequency components, i.e., $I_{sub} = \text{DWT}(I_L)$, where $sub \in \{LL, LH, HL, HH\}$, I_{LL} represents the low-frequency component, and I_{LH}, I_{HL}, I_{HH} correspond to the high-frequency components. To obtain multi-scale frequency components, we iteratively apply DWT to the low-frequency sub-image (I_{LL}), i.e., $I_{sub}^i = \text{DWT}(I_{LL}^{i-1})$, where $i \in \{1, \dots, n_i\}$, $n_i = 3$ is defined as the iteration number of DWT, $I_{sub}^i \in \mathbb{R}^{\frac{H}{2^i} \times \frac{W}{2^i} \times 3}$, and $I_{LL}^0 = I_L$.

3.3 Multi-scale Frequency Feature Extraction

Unlike Selective Stereo [37] relies on a channel-spatial attention module that implicitly learns a frequency-aware feature, we explicitly obtain the high and low frequency components of I_L by DWT. This allows that high and low frequency features can be extracted and processed separately according to different frequency properties.

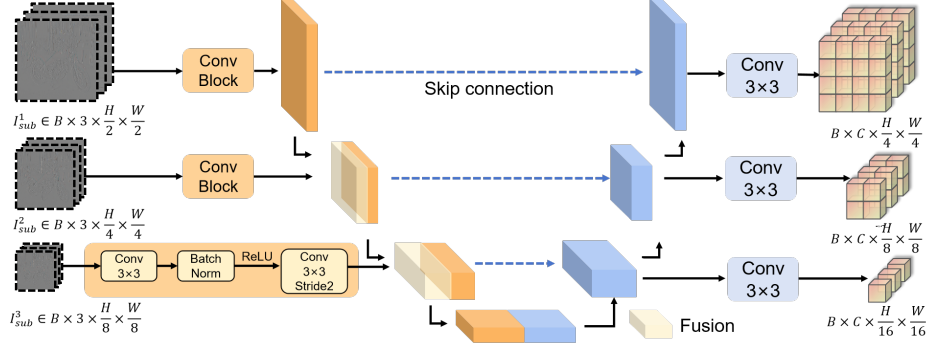


Figure 4: The framework of proposed high-frequency feature extractor consisting of a U-shaped network and a series of convolutions blocks, effectively capturing high-frequency feature through multi-scale feature aggregation and skip connection.

High-frequency Feature Extraction. To capture high-frequency details in textures, edges, and thin objects (see the second row of Fig. 2), we design a U-shaped network as the high-frequency feature extractor E_h , as shown in Fig. 4. It takes multi-scale high-frequency components I_{sub}^i ($sub \in \{LH, HL, HH\}$) and outputs multi-scale high-frequency features F_h^i , i.e., $F_h^i = E_h(I_{sub}^i)$. The resolution of F_h^i is halved by a convolutional block with a stride of 2, therefore F_h^i contains 1/4, 1/8, 1/16 scales.

Low-frequency Feature Extraction. To capture low-frequency information in smooth regions (see the third row of Fig. 2), we use the context encoder in RAFT-Stereo [25] as the low-frequency feature extractor E_l . The network consists of a series of residual blocks and downsampling layers, producing multi-scale low features F_l^i at 1/4, 1/8 and 1/16 resolution from low-frequency component I_{LL}^1 , i.e., $F_l^i = E_l(I_{LL}^1)$.

3.4 High-frequency Preservation Update Operator

Although the multi-scale high-frequency features have been sufficiently aggregated, directly incorporating them into the update operator is suboptimal, as the network focuses on different contents at different iteration stages. To address this, we propose a novel high-frequency preservation update operator (HPU) containing an iterative-based frequency adapter (IFA) and a high-frequency preservation LSTM (HP-LSTM), as shown in Fig. 5. Our IFA establishes a bidirectional interaction pathway that enables multiple rounds information fusion between the high-frequency features F_h and the current hidden state F_l , achieving adaptive feature interaction through cross-complementarity.

Iterative-based Frequency Adapter. We design two attention modules to obtain adaptive refined frequency features at different iteration steps. (1) A low-frequency selection attention (LSA) module produces structural attention maps A_l that provide global context to the high-frequency features F_h . (2) A high-frequency selection attention (HSA) module generates texture-aware attention maps A_h to inject fine details into hidden states F_l .

$$F_h^{i,j,k} = A_l^{j-1} \odot F_h^{i,j-1,k}, \quad F_l^{i,j,k} = F_l^{i,j-1,k}, \quad A_l^{j-1} = LSA(F_l^{i,j-1,k}), j \in [1, 3, 5, \dots] \quad (1)$$

$$F_l^{i,j,k} = A_h^{j-1} \odot F_l^{i,j-1,k}, \quad F_h^{i,j,k} = F_h^{i,j-1,k}, \quad A_h^{j-1} = HSA(F_h^{i,j-1,k}), j \in [2, 4, 6, \dots] \quad (2)$$

where \odot represents elementwise multiplication, i denotes the resolution dimension (1/4, 1/8, and 1/16), j is the dimension in the IFA iteration, and k is the dimension of the HPU iteration. n_j is defined as the iteration number in IFA, while n_k is defined the number of iterative updates.

High-frequency Preservation LSTM: Existing iterative-based methods employ GRU-based update operators to update the full-frequency hidden states [25, 37, 43], which results in degradation of high-frequency information during the iteration process. DLNR [51] introduces a LSTM to gradually decouple high-frequency information in updates, i.e., $F_l^k, F_h^k = LSTM(F_l^{k-1}, F_h^{k-1})$. Since we have obtained the iteration-specific high-frequency features ($F_h^{i,j,k} \neq F_h^{i,j-1,k}$) after IFA, we propose a high-frequency preservation LSTM, i.e., $F_h^{i,0,k} = F_h^{i,0,k-1}$. and inject the high-frequency features into HP-LSTM as condition (others include the correlation volume C and disparity d_{k-1}) for updating

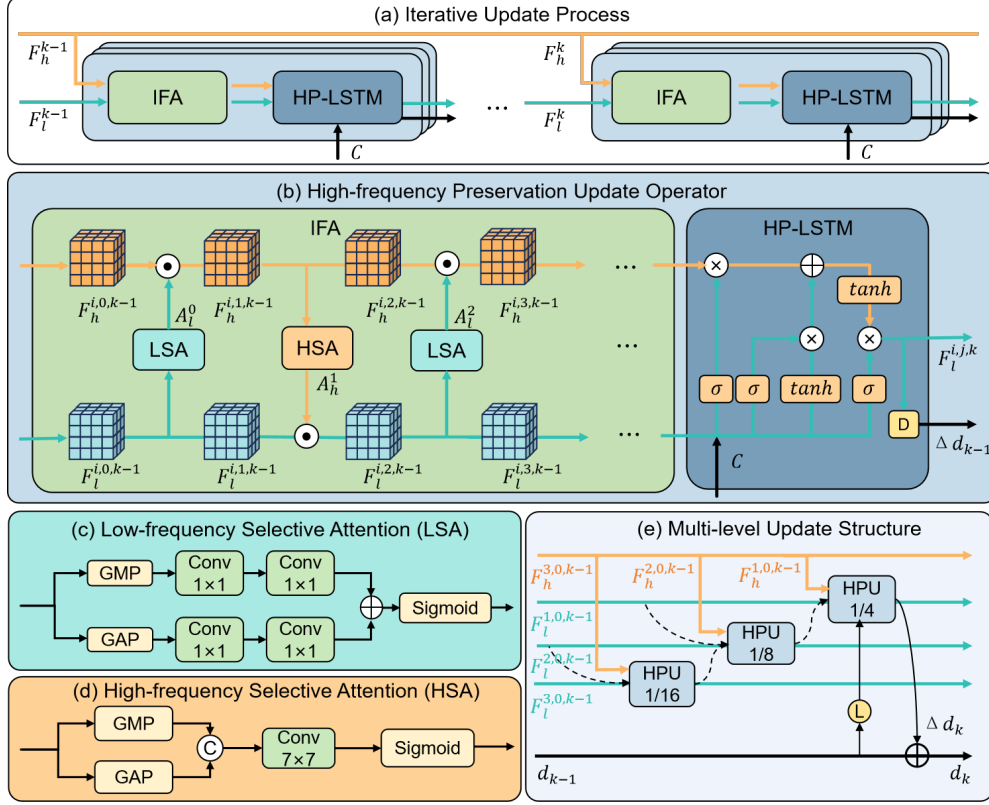


Figure 5: (a) The iterative update process of hidden states F_l , guiding by the aggregated high-frequency F_h . (b) Proposed high-frequency preservation update operator that finetunes the high-frequency in iterative-based frequency adapter and update hidden states by high-frequency preservation LSTM. (c) Low-frequency selection attention module adaptively integrates low-frequency contextual information to enhance high-frequency features (d) High-frequency selection attention module injects high-frequency attention maps to enrich low-frequency features. (e) Our multi-level update structure to update hidden states from 1/16 to 1/4.

the current hidden state F_l^k .

$$F_l^k, \Delta d_k = LSTM_{HP}(F_l^{k-1} | F_h^{k-1}, L(C, d_{k-1})) \quad (3)$$

where L refers lookup operator, the residual disparity Δd_k is decoded from the hidden state F_l^k by a decoder head D , i.e., $\Delta d_k = D(F_l^k)$. The disparity d is updated by

$$d_k = d_{k-1} + \Delta d_k. \quad (4)$$

3.5 Loss Function

We use progressively weighted L_1 loss across all predicted disparities $\{d_k\}$. Given the ground truth of disparity d_{gt} , the total loss is defined as ($\gamma = 0.9$):

$$\mathcal{L} = \sum_{k=1}^{n_k} \gamma^{n_k-i} \|d_k - d_{gt}\|_1. \quad (5)$$

4 Experiment

4.1 Implementation Details

Wavelet-Stereo is implemented in Pytorch and trained using two NVIDIA A6000 GPUs. For all experiments, we use the AdamW [26] optimizer and clip gradients to the range $[-1, 1]$. We use the

one-cycle learning rate schedule with a minimum learning rate of $2e-4$. We train Wavelet-Stereo on the Scene Flow dataset [27] as the pretrained model with a batch size of 8 and 200k iterations. The ablation experiments are trained with a batch size of 6 for 100k steps. We randomly crop images to 320×736 and use the same data augmentation as [25] for training. We use 22 update iterations during training and 32 updates for evaluation. The pipeline comparison of traditional iterative-based framework with ours is shown in Algorithm 1 and 2.

Algorithm 1 Traditional iterative framework

Require: a pair of rectified images I_L, I_R

- 1: $f_L, f_R = E_f(I_L, I_R)$
- 2: $C = \text{correlation}(f_L, f_R), d_0 = 0$
- 3:
- 4: $F_l^0 = E_l(I_L)$
- 5:
- 6: **for** $k = 1, \dots, n_k$ **do**
- 7: $F_l^k, \Delta d_k = \text{GRU}(F_l^{k-1}, \text{L}(C, d_k))$
- 8: $d_k = d_{k-1} + \Delta d_k$
- 9: **end for**
- 10: **return** disparity d

Algorithm 2 Ours

Require: a pair of rectified images I_L, I_R

- 1: $f_L, f_R = E_f(I_L, I_R)$
- 2: $C = \text{correlation}(f_L, f_R), d_0 = 0$
- 3: $I_{LL}^i, I_{HL}^i, I_{LH}^i, I_{HH}^i = \text{DWT}(I_L), i = 1, 2, 3$
- 4: $F_l^0 = E_l(I_{LL}^1)$
- 5: $F_h = E_h(\text{concat}(I_{HL}^1, I_{LH}^1, I_{HH}^1))$
- 6: **for** $k = 1, \dots, n_k$ **do**
- 7: $F_l^k, \Delta d_k = \text{HPU}(F_l^{k-1}, F_h, \text{L}(C, d_k))$
- 8: $d_k = d_{k-1} + \Delta d_k$
- 9: **end for**
- 10: **return** disparity d

4.2 Benchmark datasets and Performance

We evaluate Wavelet-Stereo on four widely used benchmarks and submit the results to online leaderboards for public comparison: KITTI 2012 [15], KITTI 2015 [28], ETH3D [33], and Scene Flow [27].

Scene Flow [27]. To verify the universality of our proposed framework, we take RAFT-Stereo and MonSter as baseline and integrate our framework. As shown in Table.1, both of our models surpass its baseline and our Wavelet-MonSter establishing a new state-of-the-art EPE benchmark on Scene Flow.

To validate the ability of our method to handle different frequency regions, we split Scene Flow test set into high-frequency region and low-frequency region with Canny operator. As shown in Tab. 3, quantitative comparisons reveal that our Wavelet-Raft outperforms Selective-RAFT on EPE metric and surpasses the baseline by 22%. Compared to Selective-IGEV [37] and DLNR [51], which is also specifically designed to address different frequency regions, our Wavelet-MonSter outperforms them by 25.89% and 10.3% in high-frequency regions, 30.2% and 13.7% in low-frequency regions, respectively.

ETH3D [33]. Following CREStereo [22] and GMStereo [37], we firstly finetune the Scene Flow pretrained model on the mixed Tartan Air [36], CREStereo Dataset [22], Scene Flow [27], Sintel

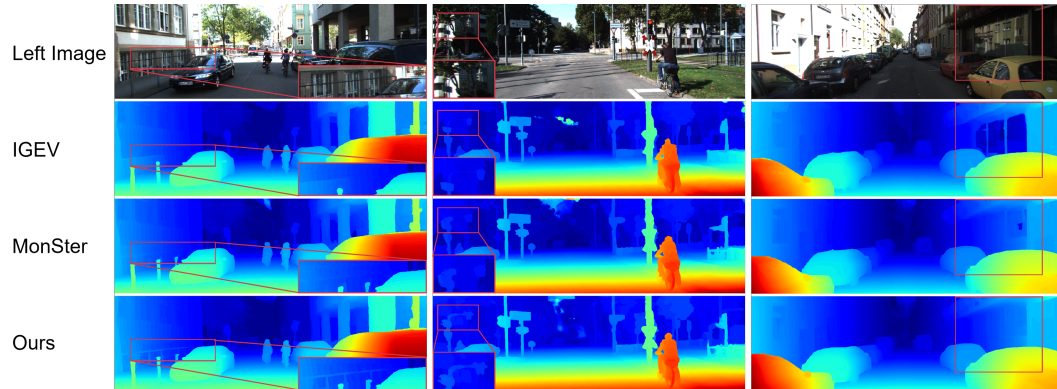


Figure 6: Qualitative results on KITTI test set. Our Wavelet-MonSter outperforms MonSter in challenging areas with high-frequency details and weak texture.

Table 1: Quantitative evaluation on Scene Flow test set. **Bold: Best**

Method	RAFT-Stereo [25]	ACVNet [42]	IGEV-Stereo [43]	Wavelet-RAFT (Ours)	MonSter [6]	Wavelet-MonSter (Ours)
EPE (px)	0.53	0.48	0.47	0.46	0.37	0.36

Table 2: Results on three popular benchmarks. All results are derived from official leaderboard publications or corresponding papers. All metrics are presented in percentages, except for RMSE, which is reported in pixels. For testing masks, “All” denotes testing with all pixels while “Noc” denotes testing with a non-occlusion mask. The **best** and **second best** are marked with colors.

	ETH3D [33]			KITTI 2015 [28]				KITTI 2012 [15]			
	Bad1.0 Noc	Bad1.0 All	RMSE Noc	D1-fg Noc	D1-all Noc	D1-fg All	D1-all All	Out-2 Noc	Out-2 All	Out-3 Noc	Out-3 All
GwcNet [17](CVPR 2019)	6.42	6.95	0.69	3.49	1.92	3.93	2.11	2.16	2.71	1.32	1.70
GANet [50](CVPR 2019)	6.22	6.86	0.75	3.37	1.73	3.82	1.93	1.89	2.50	1.19	1.60
LEAStereo [10](NeurIPS 2020)	-	-	-	2.65	1.51	2.91	1.65	1.90	2.39	1.13	1.45
ACVNet [42](CVPR 2022)	2.58	2.86	0.45	2.84	1.52	3.07	1.65	1.83	2.35	1.13	1.47
CREStereo [22](CVPR 2022)	0.98	1.09	0.28	2.60	1.54	2.86	1.69	1.72	2.18	1.14	1.46
IGEV [43](CVPR 2023)	1.12	1.51	0.34	2.62	1.49	2.67	1.59	1.71	2.17	1.12	1.44
CroCo-Stereo [38](ICCV 2023)	0.99	1.14	0.30	2.56	1.51	2.65	1.59	-	-	-	-
Selective-IGEV [37](CVPR 2024)	1.23	1.56	0.29	2.55	1.44	2.61	1.55	1.59	2.05	1.07	1.38
LoS [23](CVPR 2024)	0.91	1.03	0.31	2.66	1.52	2.81	1.65	1.69	2.12	1.10	1.38
NMRF-Stereo [16](CVPR 2024)	-	-	-	2.90	1.46	3.07	1.57	1.59	2.07	1.01	1.35
DEFOM-Stereo [20](CVPR 2025)	0.70	0.78	0.22	2.24	1.33	2.23	1.41	1.43	1.79	0.94	1.18
MonSter [6](CVPR 2025)	0.46	0.72	0.20	2.76	1.33	2.81	1.41	1.36	1.75	0.84	1.09
Wavelet-MonSter(ours)	0.44	0.68	0.20	2.60	1.31	2.60	1.38	1.32	1.71	0.83	1.07

Stereo [2], InStereo2k [1] and ETH3D [33] datasets for 300k steps. Then we finetune it on the mixed CREStereo Dataset, InStereo2k and ETH3D datasets with for another 90k steps. As shown in Tab. 2, our Wavelet-MonSter outperforms MonSter by 4.4% on Bad 1.0 metric, and achieves state-of-the-art performance among all published methods.

KITTI [15, 28]. Following the training of MonSter [6], we finetune our pretrained model on the mixed dataset of KITTI 2012 [15] and KITTI 2015 [28] with a batch size of 8 for 50k steps. For best performance, we evaluate our Wavelet-MonSter on the test set of KITTI 2012 and KITTI 2015, with results submitted to the official KITTI online leaderboard. As shown in Table.2, our Wavelet-MonSter achieves the best performance among all published approaches to date and ranks 1st on both the KITTI 2015 and KITTI 2012 leaderboards for almost all metrics, outperforming over 280 competing methods. Fig. 6 shows qualitative results on KITTI 2012 and KITTI 2015 test sets, where our Wavelet-MonSter significantly outperforms MonSter in both detailed high-frequency regions (see the first and second row of figure) and non-textured reflective regions (see the third row of figure) in the difficult scenarios.

4.3 Ablation Study

We conducted comprehensive ablation studies to validate the contribution of each component in our framework. Due to the simplified training settings, the quantitative results of ablation experiments differ from the comparison results described above. We present the main results of ablation experiments, and more results can be found in Appendix A.

Effectiveness of proposed modules. The results in the Table.4 demonstrate that it is effective and necessary to propose frequency-specific module for features with distinct convergence characteristics.

Table 3: Quantitative evaluation on Scene Flow test set in different regions (EPE).

Method	High-frequency region	Low-frequency region
RAFT-Stereo [25]	34.00	0.72
Selective-RAFT [37]	27.89	0.57
Wavelet-RAFT	26.48	0.56
DLNR [51]	31.60	0.63
Selective-IGEV [37]	26.10	0.51
MonSter [6]	26.08	0.47
Wavelet-MonSter	23.42	0.44

Table 4: Ablation study of the effectiveness of proposed modules on Scene Flow test set. HPU denotes High-frequency Preservation Update operator, F_h denotes high-frequency feature extractor.

Model	GRU	HPU	F_h	EPE (px)	D1 (%)
Baseline (RAFT-Stereo)	✓			0.62	8.40
w/o HPU	✓		✓	0.58	7.29
w/o F_h		✓		0.56	6.72
Full model (Wavelet-RAFT)		✓	✓	0.52	6.21

To assess the importance of the high-frequency feature extractor F_h , we replace F_h with a simple two-layer convolutional network. Quantitative results (EPE increases from 0.52 to 0.56) demonstrate that a powerful feature extraction network is needed to adequately fuse high-frequency information at multiple scales.

To verify the effectiveness of our proposed HPU operator, we replace it with a standard GRU module in RAFT-Stereo which simply concatenates high-frequency and low-frequency features. This modification results in performance degradation across all metrics (EPE increases from 0.52 to 0.58 and D1 increases from 6.21 to 7.29), due to GRU’s all-frequency uniform processing of different frequency features. It demonstrates that our High-frequency Preservation LSTM can flexibly utilize high-frequency information as additional conditional inputs to better balance the retention and updating of high-frequency features.

Number of IFA iteration. To determine the most appropriate interaction iteration in IFA, we conduct a systematic investigation of IFA interaction rounds by varying j from 1 to 6. As quantified in Table.5, performance exhibits a clear peak at $r=4$ iterations, with both under-interaction ($j<4$) and over-interaction ($j>4$) leading to degraded results. This suggests: (1) sufficient rounds are necessary for finetuning the iteration-specific high-frequency features, yet (2) excessive iterations may cause feature over-smoothing.

Number of Iterations. The results in the Table.6 demonstrate that our framework can significantly accelerate the speed of network convergence, which is largely attributed to the fact that we address the convergence characteristics of different frequency features separately. Specifically, providing accurate high-frequency priors in the initial iteration allows the network to focus attention on global context optimization, achieving superior performance and significantly fewer iterations than traditional iterative-based methods. Our Wavelet-RAFT need only 8 iterations to surpass the performance of RAFT-Stereo while reducing runtime by 38.6%.

Table 5: Ablation study of the rounds(j) in IFA.

Rounds (j)	EPE	Runtime(s)
1	0.394	0.680
2	0.383	0.686
3	0.371	0.772
4	0.367	0.790
5	0.371	0.865s
6	0.373	0.875s

Table 6: Ablation study of the number of iterations.

Model	Iteration	EPE	Runtime (s)
RAFT-Stereo [44]	32	0.53	0.44
	16	0.63	0.26
	12	0.53	0.22
Wavelet-RAFT	32	0.46	0.79
	16	0.47	0.45
	12	0.50	0.36
	8	0.52	0.27

5 Conclusion

We find that the underlying reason for the high-frequency degradation during the iteration process is the inconsistent convergence of the performance in the low-frequency and high-frequency regions. We propose a wavelet-based stereo matching framework (Wavelet-Stereo) for solving frequency convergence inconsistency. The core contribution is the proposed high-frequency preservation update operator, consisting of an iterative-based frequency adapter and a high-frequency preservation LSTM, which can simultaneously refine the high-frequency information at the edges and the low-frequency information in the smoothing region without losing the high-frequency information. Our novel components can be plug-and-played into multiple iterative-based methods. By processing high and

low frequency components separately, our framework can handle challenging scenes with fine details and textures in the distance. In the future, we will release a real-time version for better real-world deployment.

References

- [1] W. Bao, W. Wang, Y. Xu, Y. Guo, S. Hong, and X. Zhang. Instereo2k: a large real dataset for stereo matching in indoor scenes. *Science China Information Sciences*, 63:1–11, 2020.
- [2] D. J. Butler, J. Wulff, G. B. Stanley, and M. J. Black. A naturalistic open source movie for optical flow evaluation. In *Proceedings of the European Conference on Computer Vision*, pages 611–625. Springer, 2012.
- [3] J.-R. Chang and Y.-S. Chen. Pyramid stereo matching network. In *Proceedings of the IEEE Conference on Computer Vision and Pattern Recognition*, pages 5410–5418, 2018.
- [4] Y. Chen, H. Fan, B. Xu, Z. Yan, Y. Kalantidis, M. Rohrbach, S. Yan, and J. Feng. Drop an octave: Reducing spatial redundancy in convolutional neural networks with octave convolution. In *Proceedings of the IEEE/CVF International Conference on Computer Vision*, pages 3435–3444, 2019.
- [5] Z. Chen, W. Long, H. Yao, Y. Zhang, B. Wang, Y. Qin, and J. Wu. Mocha-stereo: Motif channel attention network for stereo matching. In *Proceedings of the IEEE/CVF Conference on Computer Vision and Pattern Recognition*, pages 27768–27777, 2024.
- [6] J. Cheng, L. Liu, G. Xu, X. Wang, Z. Zhang, Y. Deng, J. Zang, Y. Chen, Z. Cai, and X. Yang. Monster: Marry monodepth to stereo unleashes power. *arXiv preprint arXiv:2501.08643*, 2025.
- [7] J. Cheng, G. Xu, P. Guo, and X. Yang. Coatsrnet: Fully exploiting convolution and attention for stereo matching by region separation. *International Journal of Computer Vision*, 132(1):56–73, 2024.
- [8] J. Cheng, X. Yang, Y. Pu, and P. Guo. Region separable stereo matching. *IEEE Transactions on Multimedia*, 25:4880–4893, 2022.
- [9] J. Cheng, W. Yin, K. Wang, X. Chen, S. Wang, and X. Yang. Adaptive fusion of single-view and multi-view depth for autonomous driving. In *Proceedings of the IEEE/CVF Conference on Computer Vision and Pattern Recognition*, pages 10138–10147, 2024.
- [10] X. Cheng, Y. Zhong, M. Harandi, Y. Dai, X. Chang, H. Li, T. Drummond, and Z. Ge. Hierarchical neural architecture search for deep stereo matching. *Advances in Neural Information Processing Systems*, 33:22158–22169, 2020.
- [11] Z. Cheng, J. Yang, and H. Li. Stereo matching in time: 100+ fps video stereo matching for extended reality. In *Proceedings of the IEEE/CVF Winter Conference on Applications of Computer Vision*, pages 8719–8728, 2024.
- [12] S. Duggal, S. Wang, W.-C. Ma, R. Hu, and R. Urtasun. Deeppruner: Learning efficient stereo matching via differentiable patchmatch. In *Proceedings of the IEEE/CVF International Conference on Computer Vision*, pages 4384–4393, 2019.
- [13] M. Feng, J. Cheng, H. Jia, L. Liu, G. Xu, and X. Yang. Mc-stereo: Multi-peak lookup and cascade search range for stereo matching. In *2024 International Conference on 3D Vision (3DV)*, pages 344–353. IEEE, 2024.
- [14] M. Fritsche, S. Gu, and R. Timofte. Frequency separation for real-world super-resolution. In *2019 IEEE/CVF International Conference on Computer Vision Workshop (ICCVW)*, pages 3599–3608. IEEE, 2019.
- [15] A. Geiger, P. Lenz, and R. Urtasun. Are we ready for autonomous driving? the kitti vision benchmark suite. In *2012 IEEE Conference on Computer Vision and Pattern Recognition*, pages 3354–3361. IEEE, 2012.
- [16] T. Guan, C. Wang, and Y.-H. Liu. Neural markov random field for stereo matching. In *Proceedings of the IEEE/CVF Conference on Computer Vision and Pattern Recognition*, pages 5459–5469, 2024.
- [17] X. Guo, K. Yang, W. Yang, X. Wang, and H. Li. Group-wise correlation stereo network. In *Proceedings of the IEEE/CVF Conference on Computer Vision and Pattern Recognition*, pages 3273–3282, 2019.

- [18] Y.-Z. Hsieh and S.-S. Lin. Robotic arm assistance system based on simple stereo matching and q-learning optimization. *IEEE Sensors Journal*, 20(18):10945–10954, 2020.
- [19] Y. Hu, W. Wang, H. Yu, W. Zhen, and S. Scherer. Orstereo: Occlusion-aware recurrent stereo matching for 4k-resolution images. In *2021 IEEE/RSJ International Conference on Intelligent Robots and Systems (IROS)*, pages 5671–5678. IEEE, 2021.
- [20] H. Jiang, Z. Lou, L. Ding, R. Xu, M. Tan, W. Jiang, and R. Huang. Defom-stereo: Depth foundation model based stereo matching. *arXiv preprint arXiv:2501.09466*, 2025.
- [21] A. Kendall, H. Martirosyan, S. Dasgupta, P. Henry, R. Kennedy, A. Bachrach, and A. Bry. End-to-end learning of geometry and context for deep stereo regression. In *Proceedings of the IEEE International Conference on Computer Vision*, pages 66–75, 2017.
- [22] J. Li, P. Wang, P. Xiong, T. Cai, Z. Yan, L. Yang, J. Liu, H. Fan, and S. Liu. Practical stereo matching via cascaded recurrent network with adaptive correlation. In *Proceedings of the IEEE/CVF Conference on Computer Vision and Pattern Recognition*, pages 16263–16272, 2022.
- [23] K. Li, L. Wang, Y. Zhang, K. Xue, S. Zhou, and Y. Guo. Los: Local structure-guided stereo matching. In *Proceedings of the IEEE/CVF Conference on Computer Vision and Pattern Recognition*, pages 19746–19756, 2024.
- [24] Z. Liang, Y. Guo, Y. Feng, W. Chen, L. Qiao, L. Zhou, J. Zhang, and H. Liu. Stereo matching using multi-level cost volume and multi-scale feature constancy. *IEEE Transactions on Pattern Analysis and Machine Intelligence*, 43(1):300–315, 2019.
- [25] L. Lipson, Z. Teed, and J. Deng. Raft-stereo: Multilevel recurrent field transforms for stereo matching. In *2021 International Conference on 3D Vision (3DV)*, pages 218–227. IEEE, 2021.
- [26] I. Loshchilov and F. Hutter. Decoupled weight decay regularization. *arXiv preprint arXiv:1711.05101*, 2017.
- [27] N. Mayer, E. Ilg, P. Hausser, P. Fischer, D. Cremers, A. Dosovitskiy, and T. Brox. A large dataset to train convolutional networks for disparity, optical flow, and scene flow estimation. In *Proceedings of the IEEE Conference on Computer Vision and Pattern Recognition*, pages 4040–4048, 2016.
- [28] M. Menze and A. Geiger. Object scene flow for autonomous vehicles. In *Proceedings of the IEEE Conference on Computer Vision and Pattern Recognition*, pages 3061–3070, 2015.
- [29] G.-Y. Nie, M.-M. Cheng, Y. Liu, Z. Liang, D.-P. Fan, Y. Liu, and Y. Wang. Multi-level context ultra-aggregation for stereo matching. In *Proceedings of the IEEE/CVF Conference on Computer Vision and Pattern Recognition*, pages 3283–3291, 2019.
- [30] Z. Pan, J. Cai, and B. Zhuang. Fast vision transformers with hilo attention. *Advances in Neural Information Processing Systems*, 35:14541–14554, 2022.
- [31] H. Phung, Q. Dao, and A. Tran. Wavelet diffusion models are fast and scalable image generators. In *Proceedings of the IEEE/CVF Conference on Computer Vision and Pattern Recognition*, pages 10199–10208, 2023.
- [32] D. Scharstein, H. Hirschmüller, Y. Kitajima, G. Krathwohl, N. Nešić, X. Wang, and P. Westling. High-resolution stereo datasets with subpixel-accurate ground truth. In *Pattern Recognition: 36th German Conference, GCPR 2014, Münster, Germany, September 2-5, 2014, Proceedings 36*, pages 31–42. Springer, 2014.
- [33] T. Schops, J. L. Schonberger, S. Galliani, T. Sattler, K. Schindler, M. Pollefeys, and A. Geiger. A multi-view stereo benchmark with high-resolution images and multi-camera videos. In *Proceedings of the IEEE Conference on Computer Vision and Pattern Recognition*, pages 3260–3269, 2017.
- [34] Z. Shen, Y. Dai, and Z. Rao. Cfnet: Cascade and fused cost volume for robust stereo matching. In *Proceedings of the IEEE/CVF Conference on Computer Vision and Pattern Recognition*, pages 13906–13915, 2021.
- [35] Z. Shen, Y. Dai, X. Song, Z. Rao, D. Zhou, and L. Zhang. Pcw-net: Pyramid combination and warping cost volume for stereo matching. In *European Conference on Computer Vision*, pages 280–297. Springer, 2022.

- [36] W. Wang, D. Zhu, X. Wang, Y. Hu, Y. Qiu, C. Wang, Y. Hu, A. Kapoor, and S. Scherer. Tartanair: A dataset to push the limits of visual slam. In *2020 IEEE/RSJ International Conference on Intelligent Robots and Systems (IROS)*, pages 4909–4916. IEEE, 2020.
- [37] X. Wang, G. Xu, H. Jia, and X. Yang. Selective-stereo: Adaptive frequency information selection for stereo matching. In *Proceedings of the IEEE/CVF Conference on Computer Vision and Pattern Recognition*, pages 19701–19710, 2024.
- [38] P. Weinzaepfel, T. Lucas, V. Leroy, Y. Cabon, V. Arora, R. Brégier, G. Csurka, L. Antsfeld, B. Chidlovskii, and J. Revaud. Croco v2: Improved cross-view completion pre-training for stereo matching and optical flow. In *Proceedings of the IEEE/CVF International Conference on Computer Vision*, pages 17969–17980, 2023.
- [39] Z. Wu, X. Wu, X. Zhang, S. Wang, and L. Ju. Semantic stereo matching with pyramid cost volumes. In *Proceedings of the IEEE/CVF International Conference on Computer Vision*, pages 7484–7493, 2019.
- [40] B. Xu, Y. Xu, X. Yang, W. Jia, and Y. Guo. Bilateral grid learning for stereo matching networks. In *Proceedings of the IEEE/CVF Conference on Computer Vision and Pattern Recognition*, pages 12497–12506, 2021.
- [41] G. Xu, J. Cheng, P. Guo, and X. Yang. Attention concatenation volume for accurate and efficient stereo matching. In *Proceedings of the IEEE/CVF Conference on Computer Vision and Pattern Recognition*, pages 12981–12990, 2022.
- [42] G. Xu, J. Cheng, P. Guo, and X. Yang. Attention concatenation volume for accurate and efficient stereo matching. In *Proceedings of the IEEE/CVF Conference on Computer Vision and Pattern Recognition*, pages 12981–12990, 2022.
- [43] G. Xu, X. Wang, X. Ding, and X. Yang. Iterative geometry encoding volume for stereo matching. In *Proceedings of the IEEE/CVF Conference on Computer Vision and Pattern Recognition*, pages 21919–21928, 2023.
- [44] G. Xu, Y. Wang, J. Cheng, J. Tang, and X. Yang. Accurate and efficient stereo matching via attention concatenation volume. *IEEE Transactions on Pattern Analysis and Machine Intelligence*, 46(4):2461–2474, 2023.
- [45] G. Xu, H. Zhou, and X. Yang. Cgi-stereo: Accurate and real-time stereo matching via context and geometry interaction. *arXiv preprint arXiv:2301.02789*, 2023.
- [46] H. Xu and J. Zhang. Aanet: Adaptive aggregation network for efficient stereo matching. In *Proceedings of the IEEE/CVF Conference on Computer Vision and Pattern Recognition*, pages 1959–1968, 2020.
- [47] K. Xu, M. Qin, F. Sun, Y. Wang, Y.-K. Chen, and F. Ren. Learning in the frequency domain. In *Proceedings of the IEEE/CVF Conference on Computer Vision and Pattern Recognition*, pages 1740–1749, 2020.
- [48] G. Yang, X. Song, C. Huang, Z. Deng, J. Shi, and B. Zhou. Drivingstereo: A large-scale dataset for stereo matching in autonomous driving scenarios. In *Proceedings of the IEEE/CVF Conference on Computer Vision and Pattern Recognition*, pages 899–908, 2019.
- [49] N. Zenati and N. Zerhouni. Dense stereo matching with application to augmented reality. In *2007 IEEE International Conference on Signal Processing and Communications*, pages 1503–1506. IEEE, 2007.
- [50] F. Zhang, V. Prisacariu, R. Yang, and P. H. Torr. Ga-net: Guided aggregation net for end-to-end stereo matching. In *Proceedings of the IEEE/CVF Conference on Computer Vision and Pattern Recognition*, pages 185–194, 2019.
- [51] H. Zhao, H. Zhou, Y. Zhang, J. Chen, Y. Yang, and Y. Zhao. High-frequency stereo matching network. In *Proceedings of the IEEE/CVF Conference on Computer Vision and Pattern Recognition*, pages 1327–1336, 2023.

Appendix

A Dataset and evaluation metrics

Pretrain dataset: Scene Flow [27] is a synthetic stereo matching dataset consisting of 35,454 training image pairs and 4,370 testing image pairs, with a resolution of 960×540. It provides dense disparity maps as ground truth annotations for each image pair. All models in this work are trained exclusively on the SceneFlow training dataset.

Zero-shot and finetune datasets: To validate the generalization capability of our model, we evaluate its performance on the training sets of the following four real-world datasets. **KITTI 2012** [15] and **KITTI 2015** [28] are real-world driving scene datasets. Specifically, KITTI 2012 provides 194 training pairs and 195 testing pairs, while KITTI 2015 offers 200 training pairs and 200 testing pairs. **ETH3D** [33] consists of gray-scale stereo pairs acquired from diverse indoor and outdoor scenes, comprising 27 pairs for training and 20 pairs for testing. **Middlebury** [32] provides 15 training pairs and 15 testing pairs of high-resolution stereo images captured in indoor environments.

Metrics: As usual, we use end-point-error (EPE) and kpx for Scene Flow datasets evaluation metrics, where EPE is the average l_1 distance between the prediction and ground truth disparity. And kpx denotes the percentage of outliers with an absolute error greater than k pixels. Referencing previous studies, the thresholds set for each dataset are as follows: 3 pixels for KITTI-2012 and KITTI-2015, 2 pixels for Middlebury, and 1 pixel for ETH3D.

B Implementation

B.1 Implementation Details

Following [25], all models are trained with the Adam optimizer ($\beta_1 = 0.9, \beta_2 = 0.999$). For data augmentation setting, the image saturation was adjusted between 0 and 1.4, the right image was perturbed to simulate imperfect rectification that is common in datasets such as ETH3D and Middlebury. We froze all the batch normalization layers in training process. The maximum disparity D for training and evaluation is set to $D = 192$.

B.2 Frequency Convergence Inconsistency Experiment

To quantitatively evaluate frequency-specific performance, we generate edge masks using the Canny operator (implemented via OpenCV, lower=100, upper=200) on ground truth (GT) images for explicit separation of high-frequency regions and low-frequency regions. The binary edge map M serves as a high-frequency region mask, enabling calculation of high-frequency endpoint error (EPE) through element-wise multiplication:

$$EPE_{high} = M \odot EPE_{total} \quad (6)$$

Conversely, $(1 - M)$ serves as a low-frequency region mask and the low-frequency error is computed using the inverted mask $(1 - M)$:

$$EPE_{low} = (1 - M) \odot EPE_{total} \quad (7)$$

B.3 Structure of High-frequency Preservation Update Operator

The High-frequency Preservation Update Operator is consisted of Iterative-based Frequency Adapter and High-frequency Preservation LSTM.

For Iterative-based Frequency Adapter, it contains two frequency attention module: A low-frequency selection attention (LSA) module and a high-frequency selection attention (HSA) module. The LSA module processes low-frequency features carrying global structural information through a dual-path architecture. Let $F_l \in R^{H \times W \times C}$ denote the input low-frequency feature map. The module first applies both Global Max Pooling (GMP) and Global Average Pooling (GAP) along spatial dimensions to obtain channel-wise features. These pooled features then undergo channel transformation via 1×1

convolutions ($W_1, W_2 \in R^{C \times C}$) followed by *ReLU* activation function:

$$\begin{aligned} z_{max} &= \text{ReLU}[W_1(\text{GMP}(F_l))] \\ z_{avg} &= \text{ReLU}[W_2(\text{GAP}(F_l))] \\ A_L &= \sigma(z_{max} + z_{avg}) \end{aligned} \quad (8)$$

where σ denotes the sigmoid activation function.

The HSA module targets high-frequency patterns containing local textures and details. It employs identical pooling operations but processes them through a 7×7 convolutional layer W_3 to capture broader spatial contexts while suppressing noise:

$$A_H = \sigma(W_3(\text{Concat}(z_{max}, z_{avg}))) \quad (9)$$

where σ denotes the sigmoid activation function and *Concat* denotes concatenating along the channel dimension. The LSA module provides global structural context to guide high-frequency processing, while the HSA module supplies local texture details to enrich low-frequency representations.

For the High-frequency Preservation LSTM, it takes high-frequency feature F_h as condition priors along with cost volume C , disparity d_k to update the hidden states F_l :

$$\begin{aligned} x_k &= [\text{Encoder}_g(C), \text{Encoder}_d(d_k), d_k] \\ i_t &= \sigma(\text{Conv}([h_{k-1}, x_k], W_i) + b_{hi}) \\ f_t &= \sigma(\text{Conv}([h_{k-1}, x_k], W_f) + b_{hf}) \\ g_t &= \tanh(\text{Conv}([h_{k-1}, x_k], W_g) + b_{hg}) \\ o_t &= \sigma(\text{Conv}([h_{k-1}, x_k], W_o) + b_{ho}) \\ c_t &= f_t * F_h + i_t * g_t \\ F_l &= o_t * \tanh(c_t) \end{aligned} \quad (10)$$

C More Quantitative Results

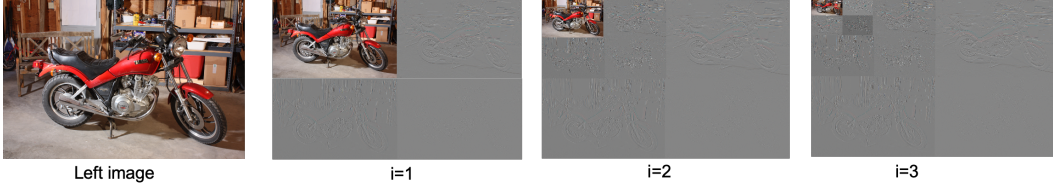


Figure 7: Different level of DWT decomposition (i refers DWT level).

Effectiveness of multi-scale high-frequency feature extractor To evaluate the efficacy of our multi-scale high-frequency feature extractor F_h , we conduct comprehensive ablation studies by feeding multi-level DWT outputs (Fig.7) into the module. It introduces only a minimal parameter increase through an efficient fusion module that aggregates multi-level high-frequency features from DWT decomposition. Quantitative evaluation on the Scene Flow test set (Table. 7) demonstrates that this lightweight design adds just 0.77M additional parameters while achieving 2.3% improvements (EPE decreases from 0.483 to 0.472).

Table 7: Ablation studies of the effectiveness of our multi-scale high-frequency feature extractor. 1, 2, 3 stand for the level of Discrete Wavelet Transform (DWT).

Method	EPE	D1	Params. (M)
HPU	0.563	6.92	0.55
HPU + HAM ₁	0.483	6.39	4.36
HPU + HAM ₂	0.472	6.26	4.73
HPU + HAM ₃ (Ours)	0.467	6.21	5.5

Our high-frequency feature extractor which is fed 3-level DWT decomposition outputs achieves effective fusion and utilization of multi-scale high-frequency features. This carefully balanced design

Table 8: Computational complexity breakdown per stage. Runtime, GPU memory usage, number of parameters, and equivalent FPS are reported.

Stage	Memory(MB)	Params(M)	Runtime(ms)
DWT	0	-	33.31
Low-frequency Feature Extraction	1660	4.32	10.65
High-frequency Feature Extraction	2064	7.01	5.44
Cost volume	2072	-	70.54
HPU-Refinement	2178	6.47	369.16

maintains the model’s compactness and practical deployability while enabling effective multi-scale high-frequency feature utilization.

Parameter and Computational Analysis We further provide quantitative results on memory usage and computational cost. We use a single Nvidia A6000 graphics card (with 48 GiB memory) and the batch size is set to 1 for the inference (16 iterations). The memory consumption and computational cost is shown in Table.8

D More Qualitative Results

In this section, we provide a comprehensive qualitative comparison between our method and the baselines on four widely used real-world datasets (KITTI 2012 [15], KITTI 2015 [28], Middlebury [32] and ETH3D [33]). As shown in Fig.10, Fig.8, Fig.11 and Fig.9, our Wavelet-RAFT exhibits significantly superior zero-shot generalization performance compared to baseline model when pretrained exclusively on the synthetic SceneFlow [27] dataset. Our Wavelet-MonSter demonstrates remarkable performance in preserving hierarchical details in the predicted disparity maps, with even the most delicate structures being accurately maintained, as shown in Figure. 12.

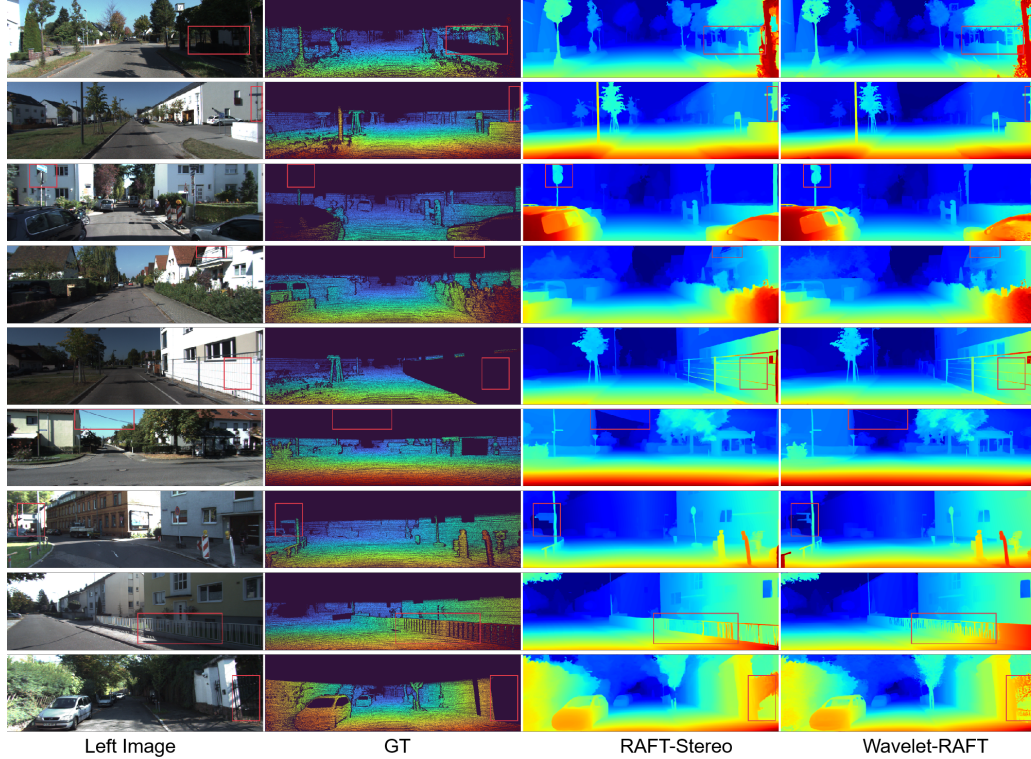


Figure 8: **Qualitative Results – Zero-Shot Generalization on the KITTI 2012 and KITTI 2015 train sets.**

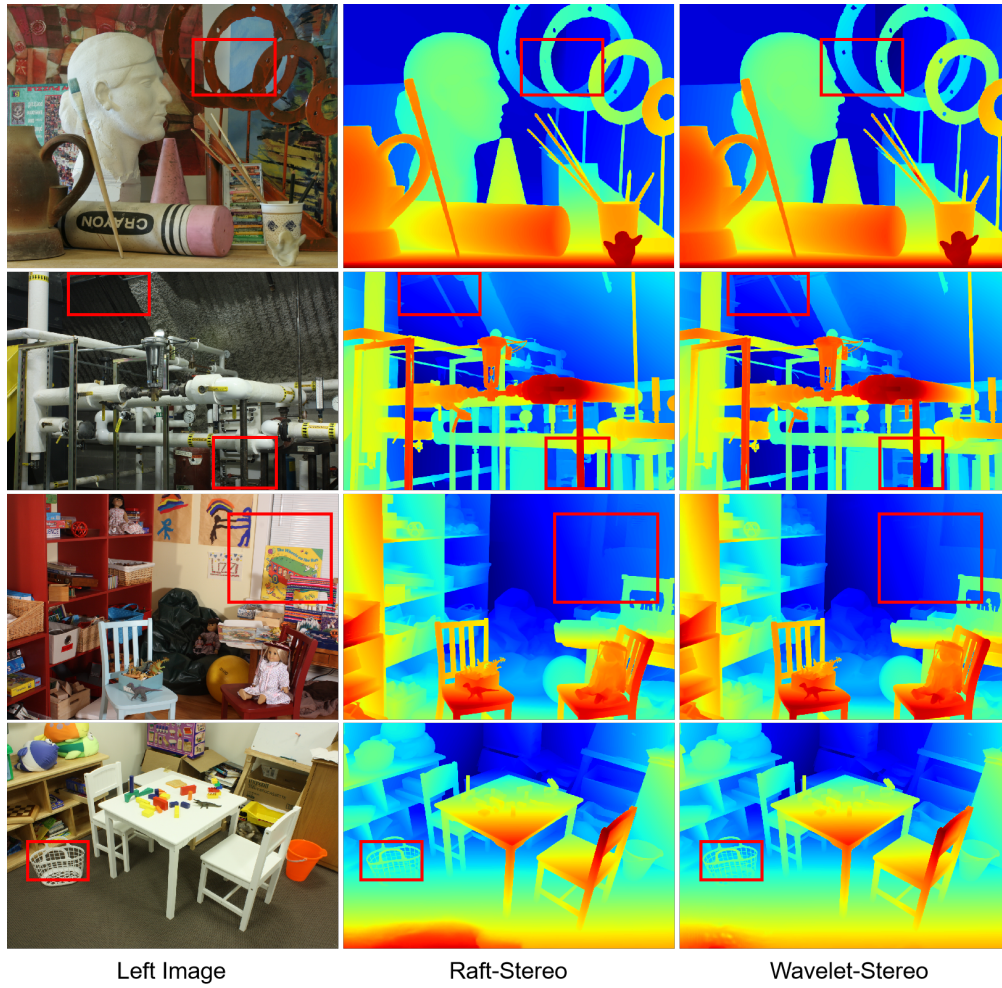


Figure 9: Qualitative Results – Zero-Shot Generalization on the Middlebury [32] train set.

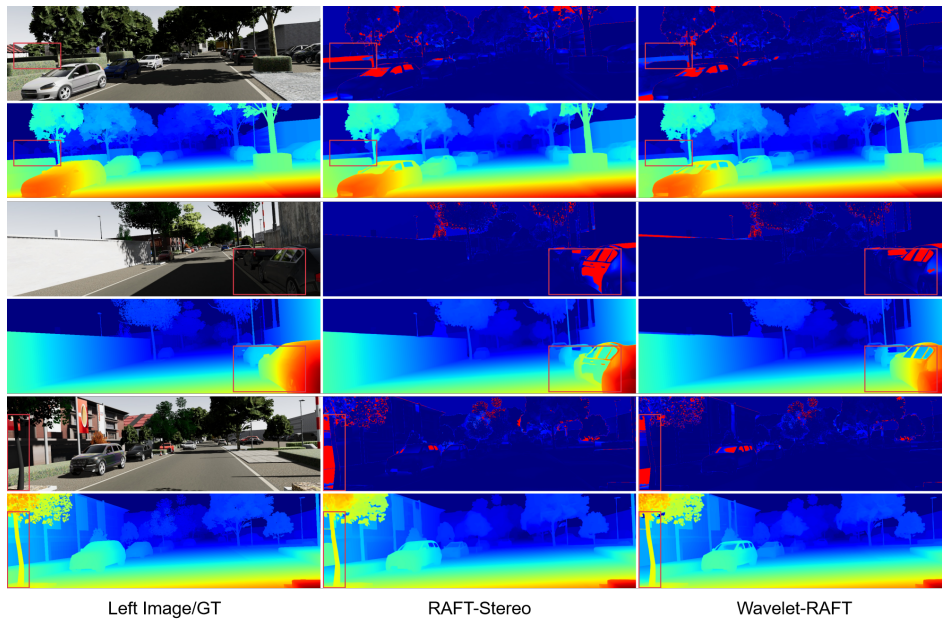


Figure 10: Qualitative results on VKITTi train set. The first column shows the left image and the corresponding ground-truth disparity map. The rest columns show the error map and the predicted disparity map of RAFT-Stereo and Wavelet-RAFT, respectively.

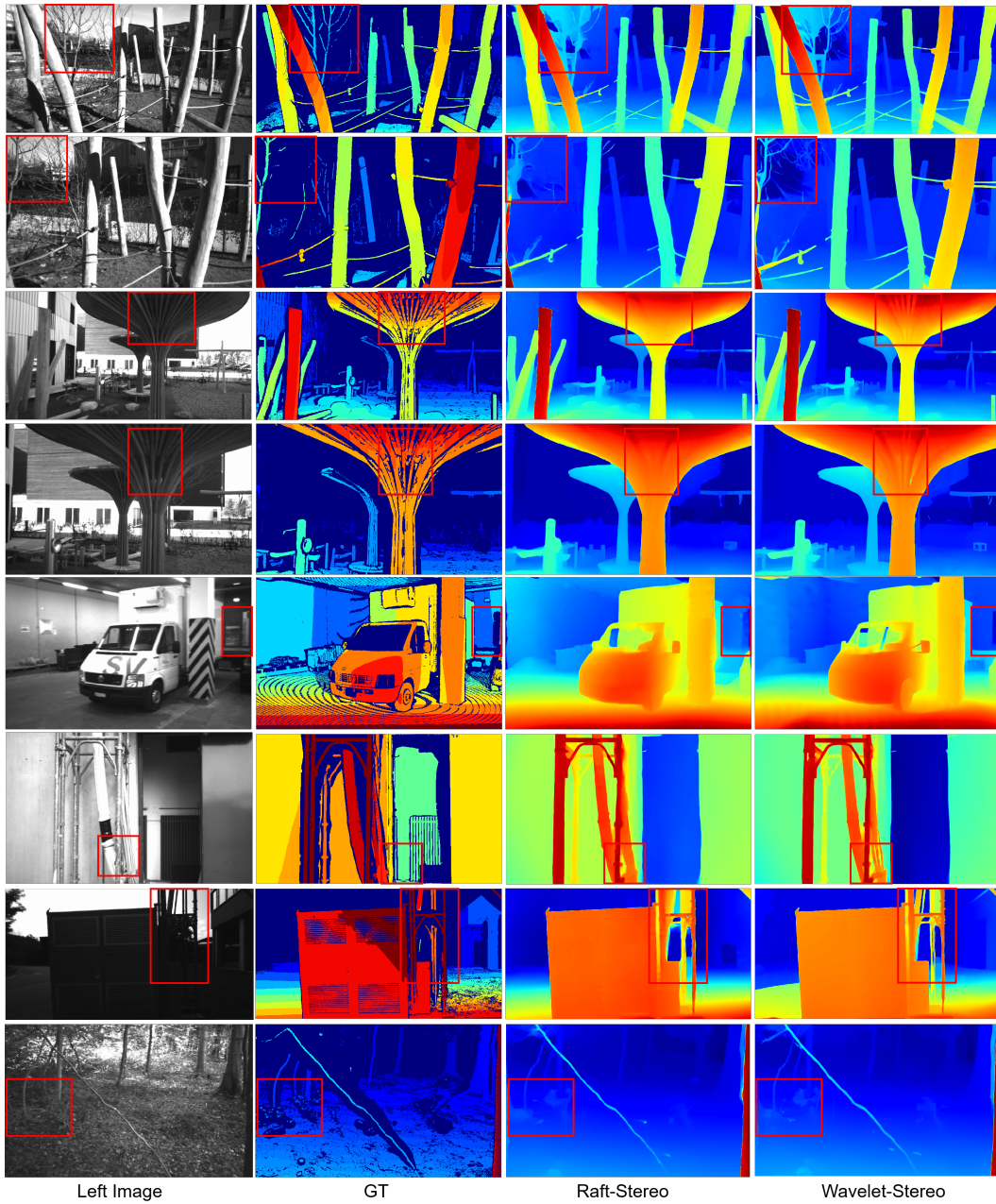


Figure 11: Qualitative Results – Zero-Shot Generalization on the ETH3D [33] train set

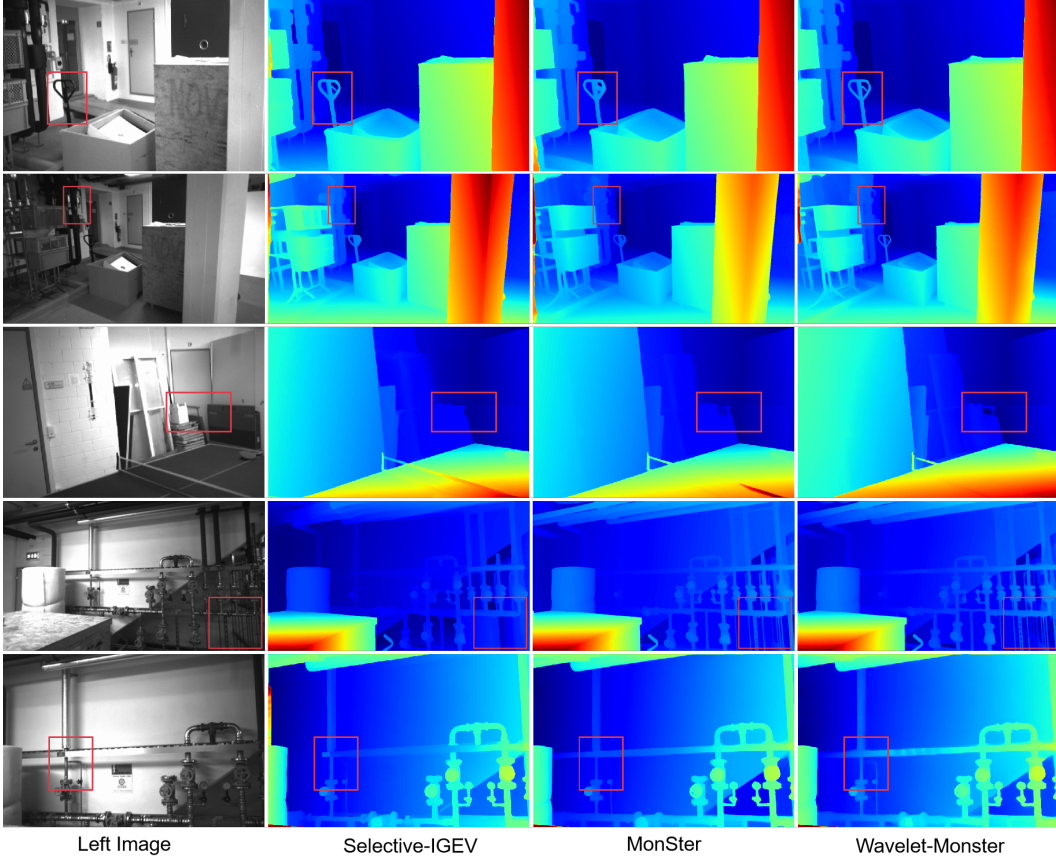


Figure 12: Qualitative results on ETH3D test set.

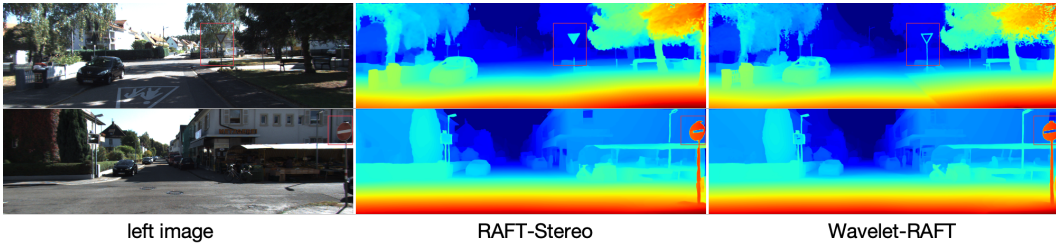


Figure 13: Examples of failure cases for the proposed method. Poor performance due to unnecessary extraction of task-irrelevant information.

E Discussions, Limitations, and Further Work

Limitations. While the proposed method demonstrates strong performance, the computational overhead induced by the DWT decomposition, multi-scale feature extraction, and iterative frequency adapter (IFA) operations could potentially hinder real-time deployment. These limitations highlight important trade-offs between frequency-aware precision and computational practicality that warrant further investigation in future work.

Further Work. Here are some directions of our future work.

1. Semantics-guided high-frequency processing pipeline that discriminatively extracts task-relevant high-frequency information.
2. Adaptive number of iteration for different scenarios.
3. Exploring the application of diffusion model in stereo matching.